Development of Intrinsic Properties and Excitability of Layer 2/3 Pyramidal Neurons During a Critical Period for Sensory Maps in Rat Barrel Cortex

Miguel Maravall, Edward A. Stern, and Karel Svoboda

Howard Hughes Medical Institute, Cold Spring Harbor Laboratory, Cold Spring Harbor, New York 11724

Maravall, Miguel, Edward A. Stern, and Karel Svoboda. Development of intrinsic properties and excitability of layer 2/3 pyramidal neurons during a critical period for sensory maps in rat barrel cortex. *J Neurophysiol* 92: 144–156, 2004; 10.1152/jn.00598.2003. The development of layer 2/3 sensory maps in rat barrel cortex (BC) is experience dependent with a critical period around postnatal days (PND) 10–14. The role of intrinsic response properties of neurons in this plasticity has not been investigated. Here we characterize the development of BC layer 2/3 intrinsic responses to identify possible sites of plasticity. Whole cell recordings were performed on pyramidal cells in acute BC slices from control and deprived rats, over ages spanning the critical period (PND 12, 14, and 17). Vibrissa trimming began at PND 9. Spiking behavior changed from phasic (more spike frequency adaptation) to regular (less adaptation) with age, such that the number of action potentials per stimulus increased. Changes in spiking properties were related to the strength of a slow Ca^{2+}-dependent afterhyperpolarization. Maturation of the spiking properties of layer 2/3 pyramidal neurons coincided with the close of the critical period and was delayed by deprivation. Other measures of excitability, including *I-f* curves and passive membrane properties, were affected by development but unaffected by whisker deprivation.

INTRODUCTION

The development of neuronal circuits in the neocortex is dependent on prior experience and activity (Katz and Shatz 1996). This developmental plasticity could involve many mechanisms, most of which we understand poorly (Crair and Malenka 1995; Fox 1995; Hensch et al. 1998; Huang et al. 1999; Kirkwood et al. 1995; Lu et al. 2001; Philpot et al. 2001; Quinlan et al. 1999). The barrel cortex of rodents is an ideal system for studying experience-dependent cortical development (Fox 1992; Simons and Land 1987). A topographical sensory map from the vibrissae (whisker) pad to primary somatosensory cortex (S1) is established during development. Barrels are discrete aggregates of neurons in layer 4 (Welker and Woolsey 1974; Woolsey and Van der Loos 1970) that correspond to representations of particular vibrissae: neurons in a barrel and the adjacent supra- and infragranular regions respond preferentially to a principal whisker (PW) (Armstrong-James and Fox 1987; Simons 1978; Welker 1971). Whiskers surrounding the PW provide weaker and slower inputs (Armstrong-James and Fox 1987; Armstrong-James et al. 1991; Fox 1994; Moore and Nelson 1998; Zhu and Connors 1999). Thus in animals raised with normal sensory experience, the electrophysiological map mirrors the anatomical map. Barrels form soon after birth (Schlaggar and O'Leary 1994) and are resistant to sensory manipulation after an early critical period [postnatal day (PND) 5] (Fox et al. 1996; Henderson et al. 1992; Rice and Van der Loos 1977). However, sensory deprivation by whisker clipping can continue to modify receptive fields in a layer-specific manner (Armstrong-James et al. 1994; Diamond et al. 1994; Fox 1992; Glazewski and Fox 1996; Hand 1982; Lendvai et al. 2000; Simons and Land 1987).

We recently analyzed layer 2/3 subthreshold whisker receptive fields using in vivo intracellular recordings from PND 14 to PND 20 (Stern et al. 2001). We found that trimming all contralateral whiskers from PND 9 disrupted receptive fields: responses to PW stimulation decreased significantly, while surround responses increased. This plasticity had a critical period: deprivation at PND 15 failed to disrupt receptive fields measured at PND 20. Layer 4 responses showed no deprivation-induced changes after clipping from PND 9, ruling out a prominent role for thalamocortical plasticity in layer 2/3 sensory map modification.

The mechanisms underlying this critical period for plasticity and its closure are unknown. Developmental changes in long-term potentiation (LTP) could be involved (Crair and Malenka 1995; Feldman et al. 1998; Isaac et al. 1997; Kirkwood et al. 1995). However, synaptic inputs to layer 2/3 are overwhelmingly intracortical (Armstrong-James et al. 1992; Feldmeyer et al. 2002; Laaris et al. 2000; Petersen and Sakmann 2001), and LTP at these synapses persists past the critical period (Allen et al. 2003; Feldman 2000; Maravall and Svoboda, unpublished observations). Intracortical synaptic density increases several-fold between PND 9 and 15 (De Felipe et al. 1997; Micheva and Beaulieu 1996), implying that synaptic circuits could change rapidly. Indeed, experience-dependent turnover of dendritic spines (Lendvai et al. 2000; Trachtenberg et al. 2002) and dendritic branches (Maravall et al. 2004) suggests that experience-dependent formation and elimination of synapses is involved in experience-dependent plasticity.

Another locus of plasticity could be the intrinsic excitability and input-output relationships of neurons (reviewed in Zhang and Linden 2003). Intrinsic properties including spike generation thresholds and various ionic conductances can be modified by experience (Aizenman et al. 2003; Disterhoft et al. 1986; Saar and Barkai 2003; Schreurs et al. 1998) and by manipulation of activity levels in vitro (Aizenman and Linden 2000; Armano et al. 2000; Daoudal et al. 2002; Desai et al. 1999; Franklin et al. 1992; Ganguly et al. 2000; Garcia et al. 1994; Li et al. 1996; Nelson et al. 2003; Nick and Ribera 2000; Sourdet et al. 2003; Turrigiano et al. 1994). It is unknown whether such activity-dependent modifications of intrinsic properties might

---

contribute to the developmental plasticity of cortical somato-sensory responses. We therefore measured the development of intrinsic excitability and spiking properties of excitatory neurons in layers 2/3 and 4 during the critical period mentioned (PND 12–17), using whole cell patch-clamp recordings in an acute barrel cortex (BC) slice preparation. Maturation of excitability and of spiking properties occurs in layer-specific fashion. Sensory deprivation induced by full contralateral whisker clipping delays maturation of spiking properties. These changes in spiking behavior correlate with changes in a Ca^{2+}-dependent slow afterhyperpolarization (AHP). Deprivation does not affect intrinsic excitability as measured by I-f curves.

METHODS

Animal-deprivation protocol

All procedures were undertaken in accordance with animal care and use guidelines of Cold Spring Harbor Laboratory. Rat pups were deprived by clipping all whiskers on one side of the snout to <1 mm length, starting at age PND 9 and continuing at intervals of <48 h (recordings were made at PND 12, 14, and 17). Clipping was performed with no anesthesia and brief handling; control animals were also handled during clipping sessions. Deprived animals were kept in the same cages as their mothers and control littermates until the experiment. The experimenter was blind to animal deprivation history until after the experiment's analysis was completed.

Electrophysiology

Neocortical brain slices were prepared from the hemisphere contralateral to the clipped whiskers. The brain was removed and blocked at an angle intermediate between coronal and sagittal (40-45° from the midline, anteromedial to posterolateral) and inclined ~10° from the vertical plane. This angle was approximately parallel to barrel arcs (Feldman 2000; Finnerty et al. 1999; Shepherd et al. 2003). The most posterior slices showing barrels under bright-field illumination were then those containing the large barrels of the posterior medial barrel subfield (PMBSF), corresponding to the longer vibrissae at the posterior edge of the whisker pad. Slices (300 μm thick) were cut on a VT-100 microtome (Leica, Wetzlar, Germany) with the brain submerged in a chilled (2-5°C) cutting solution bubbled with carbogen (95% O_2-5% CO_2). The solution contained (in mM) 110 choline-chloride, 25 $NaHCO_3$, 25 D-glucose, 11.6 Na-ascorbate, 7 $MgSO_4$, 3.1 Na-pyruvate, 2.5 KCl, 1.25 NaH_2PO_4, and 0.5 $CaCl_2$. After cutting, slices were transferred to a submerged holding chamber containing artificial cerebrospinal fluid (ACSF) and incubated at 35°C for 25-50 min, and then held at room temperature until used. The composition of the normal ACSF was (in mM) 127 NaCl, 25 $NaHCO_3$, 25 D-glucose, 2.5 KCl, 2 $CaCl_2$, 1 $MgSO_4$, and 1.25 NaH_2PO_4. All chemicals were from Sigma (St. Louis, MO) unless otherwise noted. Drugs (TTX, $CdCl_2$, 4-aminopyridine) were routinely added to the bath perfusion.

Recordings were performed only within slice regions that contained barrels of the PMBSF identified under transillumination. Neurons were identified visually and selected for whole cell recording using IRDIC optics. Cells were selected according to morphology (pyramidal if in layer 2/3, stellate if in layer 4) and position. Layer 2/3 pyramids were 200-300 μm from the pia; this helped to limit the variability across cells at different depths (Peters and Jones 1984). Neurons with transversal apical arbors (usually adjacent to layer 1) were not used (van Brederode et al. 2000).

Experiments were performed at 34 ± 1°C (mean ± SD). Patch electrodes (3-6 MΩ) were filled with an internal solution containing (in mM) 135 K^+-methylsulfonate, 10 HEPES, 10 Na-phosphocre-atine, 4 $MgCl_2$, 4 Na_2-ATP, and 0.4 Na-GTP. For calcium imaging experiments, the 1,2-bis(2-aminophenoxy) ethane-N,N,N',N'-tetraacetic acid (BAPTA)–based dye Oregon Green BAPTA-1 (OGB-1; 40 or 100 μM, Molecular Probes, Eugene, OR) was added to the solution.

Electrophysiological data acquisition was performed using an Axopatch 200B amplifier (Axon) and software written in Igor (Wavemetrics). Data were sampled at 4-kHz resolution. For imaging, we used a custom-built two-photon laser-scanning microscope (Mainen et al. 1999; Maravall et al. 2000). Acquisition protocols began 1-2 min after break-in to whole cell configuration. During calcium imaging experiments, immediately on breaking into whole cell mode, a position was found on the proximal apical dendrite. Laser scanning was then changed from frame-scan, two-dimensional mode to line-scan mode over a one-dimensional line across the dendrite. Calcium imaging began ~2 min after break-in and ended when loading approached a steady state ≤40 min later (Maravall et al. 2000).

Stimuli were delivered in current clamp mode. To construct current-frequency curves (Fig. 2), square pulses (500-ms duration) were given in increases of 50 pA; currents ranged from 50 to 700-1,000 pA. Individual action potentials (APs) were evoked using short (2-5 ms) current pulses: to characterize afterhyperpolarizing potentials, AHPs, APs were evoked either individually or as sequences of 10 pulses at 100 Hz (Fig. 3A). To calibrate $[Ca^{2+}]$ from fluorescence recordings, sequences of 40-50 (83 Hz) or 48-60 (100 Hz) APs were interleaved with single APs (Maravall et al. 2000).

Electrophysiology analysis and $[Ca^{2+}]$ calibration

Electrophysiology and calcium-imaging analyses were carried out using custom software (written in Igor). Neurons were classified as phasic or regular-spiking depending on whether they could spike throughout the duration of 500-ms-duration depolarizing current pulses. If a neuron could spike throughout, it was scored as regular. If it never fired spikes in the last 200 ms of a 500-ms pulse of any current size, it was phasic. For further analysis of spiking behavior we used the "spike ratio, R," defined as the number of spikes fired during the second 100 ms of a stimulus, divided by the number of spikes fired during the first 100 ms. R was only measured for responses with two or more spikes. To compare R across experiments, we used the maximal R collected during the experiment. This was consistent with our scheme for scoring neurons as RS or PS.

Action potentials were characterized by their threshold as measured at the inflection point, by their height (from threshold to peak) and by their width measured at half-maximum height. Our results may underestimate the magnitude of age-related increases in AP amplitude and decreases in AP duration due to our use of the Axopatch 200B amplifier, which is not an optimal voltage follower.

Voltage deflections evoked by 500-ms current pulses were measured at plateau level (for positive currents) and at peak and plateau level (for negative currents). Sag potentials measured with negative current steps were computed as the difference between peak deflection and plateau deflection. Rebound potentials occurring on negative pulse offset were also analyzed and their comparison gave similar results to sag potentials. Current-voltage (I-V) curves were computed using subthreshold stimulation intensities. For negative currents, inward rectification was measured at peak deflection, giving an estimate of the relative strength of fast inwardly rectifying currents. For positive currents, outward rectification was measured only in experiments where APs were abolished by TTX (Fig. 4). In such cases, both early and late outward rectification were measured. Input impedances were measured in voltage clamp using single-exponential fits to a current step, and in current clamp by determining the slope of the current-voltage curve at small negative currents (−100-0 pA). Current-frequency (I-f) curves were constructed and smoothed (3-point boxcar).

Line-scan $[Ca^{2+}]$ fluorescence images were averaged across dendrite width (determined as the full width at half-maximum fluores-
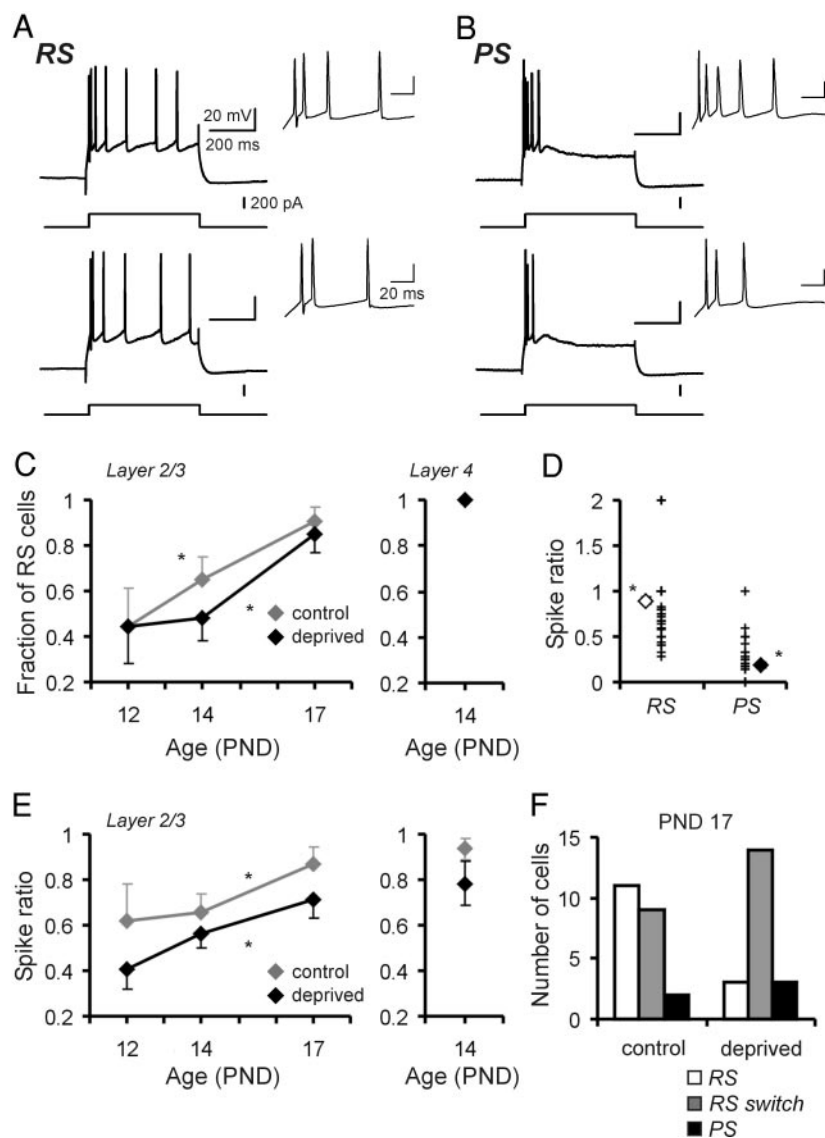
FIG. 1. Maturation of layer 2/3 pyramidal cell spiking behavior. *A*: regular spiking (RS) responses recorded in a postnatal day (PND) 14 cell. *Top panels*: voltage response (top) and stimulus trace for a 400-pA current pulse (500-ms duration). *Bottom panels*: response and stimulus for a 300-pA current pulse. Spiking behavior did not depend on stimulus intensity. *Insets*: earliest part of voltage response for the same traces. *B*: phasic spiking (PS) patterns from a different PND 14 cell. Spiking behavior was not dependent on stimulus intensity (all panels as for *A*). *C*: fraction of RS cells varies as a function of age and condition. In layer 2/3, the majority of younger (PND 12) neurons had PS responses, while at PND 17 most neurons had RS responses. In layer 4, all cells were RS already by age PND 14. Experience delayed the maturation process (asterisks indicate significant difference between curves). In gray: control, in black: deprived. *D*: spike ratio *R* (number of spikes fired 100-200 ms into pulse divided by number of spikes fired 0-100 ms into pulse) is highly correlated with spiking behavior as scored by experimenter. Open: RS, filled: PS. *E*: spike ratio *R* varies as a function of age and condition (asterisks indicate significant difference between curves). Developmental time course was very similar to that of RS behavior. Key as for *C*. *F*: relative numbers of RS, RS switching and PS neurons at PND 17 are affected by deprivation.

cence). Resting fluorescence was averaged over the 64-128 ms preceding AP stimulation. Peak amplitudes of fluorescence transients were calculated by averaging over 15 ms for single stimuli or over a 100- to 120-ms plateau for saturating transients evoked by AP trains. The only background signal that was subtracted was that due to PMT dark currents (Sabatini et al. 2002). To enable calibration of fluorescence transients in terms of absolute $[Ca^{2+}]$, the high-affinity indicator OGB-1 was chosen. OGB-1 saturates at comparatively low $[Ca^{2+}]$ increases ($K_D \approx 205$ nM). To measure resting calcium ($[Ca^{2+}]_0$), action potential-evoked Ca^{2+} transients ($\Delta[Ca^{2+}] = [Ca^{2+}] - [Ca^{2+}]_0$), and the buffering capacity of internal calcium buffers (κ), we used previously published methods (Maravall et al. 2000; Sabatini et al. 2002).

RESULTS

Development of electrophysiological properties

We compared functional properties of layer 2/3 pyramidal neurons and layer 4 spiny stellate neurons from the BC of control and deprived rats at PND 12, 14, and 17. Whole cell patch recordings in current-clamp mode (Fig. 1) were performed in pyramidal and spiny stellate cells from slices of BC.

Characterization of spiking behavior was performed in a total of $n = 162$ neurons, all of which had resting potentials more negative than −55 mV, had overshooting APs and were able to fire repeatedly in response to depolarizing current pulses. Subgroups of these recordings were used for additional experimental protocols and analyses.

Spiking behavior

On stimulation with a square current pulse (500 ms) delivered through the patch pipette, most cells from older (≥PND 14) animals responded with the regular-spiking (RS; Fig. 1*A*) patterns typical of mature supragranular pyramidal neurons (Amitai and Connors 1995; Connors and Gutnick 1990; McCormick et al. 1985). RS neurons have moderate spike-frequency adaptation (SFA): they continue to fire throughout the stimulation pulse. However, pyramidal cells from younger animals often showed phasic-spiking (PS; Fig. 1*B*) patterns with complete SFA. In these neurons, there were never any spikes in the last 200 ms of a 500-ms pulse. PS and RS spiking patterns are easily classified and completely distinct (see METH-
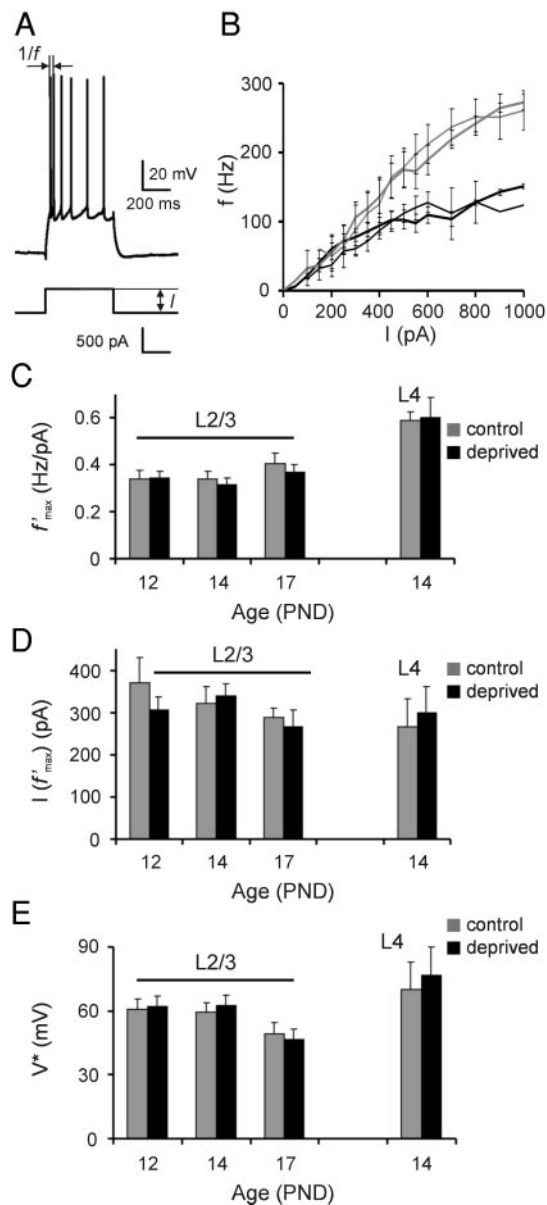
FIG. 2. Intrinsic response properties of layer 2/3 pyramidal cells. *I-f* curves changed with maturation and were different across layers but were unaffected by deprivation. *A*: measurement of instantaneous excitability via response frequency on stimulation. A current pulse of size *I* produced a response at frequency *f*. *B*: in vitro current-frequency (*I-f*) curves averaged for each condition, PND 14 neurons. In gray: layer 4 cells; in black: layer 2/3 neurons; thick line: control condition, thin line: deprived condition. Experiments averaged: $n = 6$ (layer 4 control), $n = 4$ (layer 4 deprived), $n = 12$ (layer 2/3 control), $n = 10$ (layer 2/3 deprived). *C*: maximum slope f'_{max} by layer, age, and condition. Gray columns: control, black columns: deprived. Layer 2/3 and 4 groups are indicated over bars. *D*: current of maximum slope $I(f'_{max})$, by layer, age, and condition. Colors as for *C*. *E*: maximum slope scaled voltage $V*$, by layer, age, and condition. Colors as for *C*. Number of experiments averaged in *D–E*: for layer 2/3, $n = 9$-10 (PND 12 control), $n = 9$ (PND 12 deprived), $n = 11$-13 (PND 14 control), $n = 10$ (PND 14 deprived), $n = 8$ (PND 17 control), $n = 6$ (PND 17 deprived); for layer 4, $n = 6$ (PND 14 control), $n = 4$ (PND 14 deprived).

ODS). Phasic spiking patterns have been observed previously in vitro in immature excitatory neurons from various cortical regions (Locke and Nerbonne 1997; Lorenzon and Foehring 1993; Metherate and Aramakis 1999) and also in vivo (Dégenètais et al. 2002). They differ from the stereotyped burst

responses shown by intrinsically bursting pyramidal neurons in layer 5. Because the more mature RS neurons sustain spiking for longer, they can potentially generate a larger number of APs in response to a stimulus.

We scored cells according to their characteristic spike patterns as either regular or phasic spiking (RS or PS). The fraction of RS cells in layer 2/3 increased gradually with age both in control and deprived animals (Fig. 1*C*), progressing from 44% ($n = 4$ of 9) in both conditions at PND 12, through 65% of control cells ($n = 15$ of 23) and 48% of deprived cells ($n = 12$ of 25) at PND 14, to 91% of control cells ($n = 20$ of 22) and 85% ($n = 17$ of 20) of deprived cells at PND 17. Therefore expression of mature spiking patterns is essentially complete at PND 17, by the end of the critical period for sensory response plasticity in layer 2/3 (Stern et al. 2001).
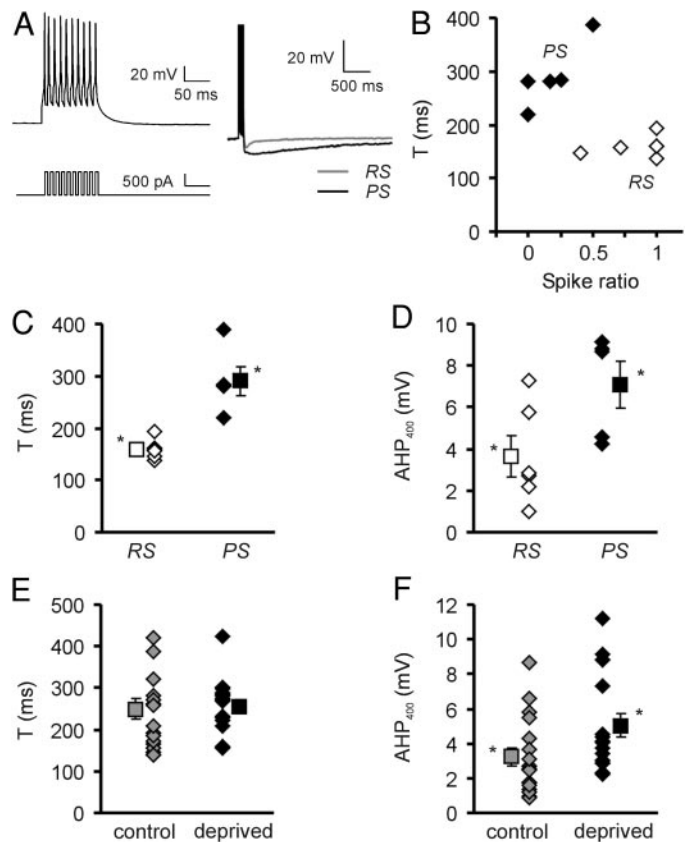

FIG. 3. Slow afterhyperpolarization (AHP) and spiking behavior. *A*: cells with different spiking patterns showed different slow AHPs, although not necessarily different fast- and medium-duration AHPs. *Left*: example of protocol used to analyze AHP, using a 100-Hz train of 10 APs. *Right*: superposed examples of RS and PS responses from 2 different neurons showing difference in AHP waveform. In gray: RS neuron; in black: PS neuron. Voltage traces (*top*) were cut off at 0 mV for greater magnification. Note that for the PS neuron (but not the RS neuron), the slow AHP peak is also the overall AHP peak. *B*: time *T* to overall AHP peak for PND 17 RS and PS neurons plotted against spike ratio *R*. Data fell into 2 groups that agreed with spiking behavior as scored by experimenter. *C*: time *T* to overall AHP peak for PND 17 RS and PS neurons. Open: RS cells, filled: PS cells. Diamonds: individual experiments. Squares: averages. (Error bars across RS cells are smaller than the size of the square.) Asterisks denote significant difference. *D*: AHP amplitude 400 ms after the end of the pulse train for PND 17 RS and PS neurons. Color key as for *B*. Asterisks: significant difference. *E*: time *T* to overall AHP peak for PND 17 control and deprived neurons. In gray: control, in black: deprived. Diamonds: individual experiments. Squares: averages. *F*: AHP amplitude 400 ms after the end of the pulse train for PND 17 control and deprived neurons. Key as for *E*. Asterisks: significant difference.
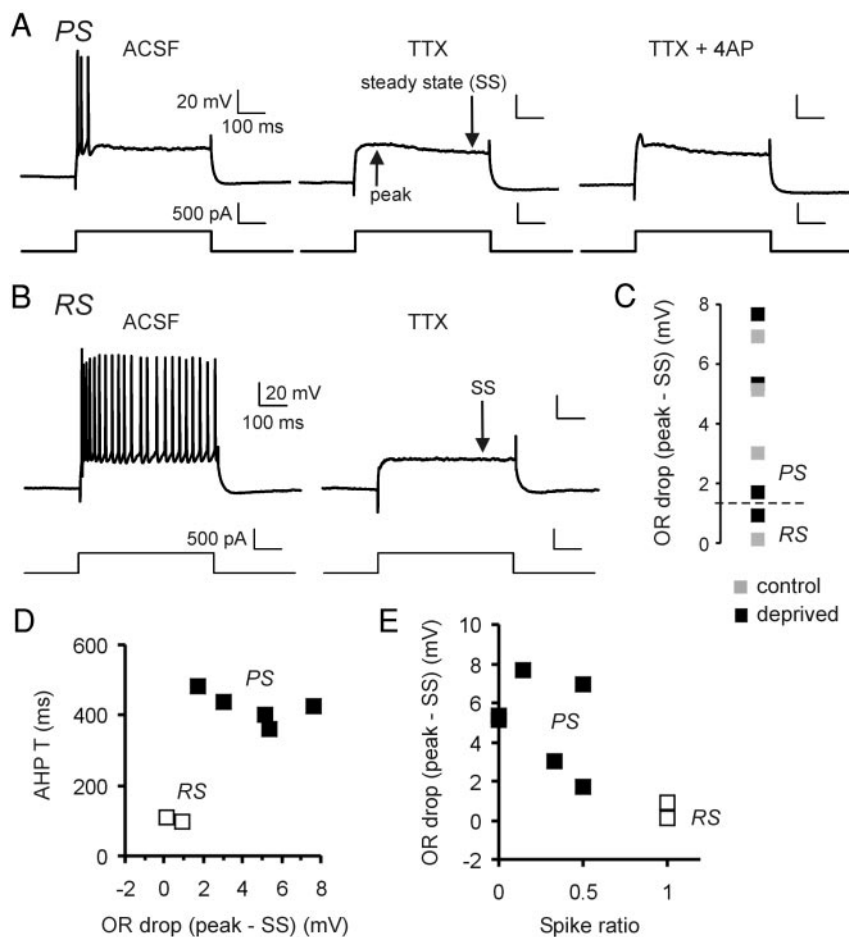
FIG. 4. Subthreshold late outward rectification (OR) and spiking behavior. (All data recorded from PND 14 slices). *A*: traces from a PS cell showing responses to a 500-pA current pulse in drug-free artificial cerebrospinal fluid (ACSF; *left*), in 1 μM TTX (*middle*), and in TTX plus 50 μM 4AP (*right*). "Steady state" (SS) indicates the time when a response reached a stable value. Note how (*right*) 4-aminopyridine (4-AP) did not affect the SS response but, instead, allowed appearance of a distinctive earlier depolarizing peak. *B*: equivalent traces from an RS cell (500-pA current pulse) in ACSF (*left*) and in 1 μM TTX (*right*). Note the large late OR in the PS response (*A*) as compared with the RS response, even in the absence of action potential (AP) activity. Key as for *A*. *C*: late OR voltage drop in the presence of TTX: depolarization at the pulse end (SS, averaged 450-500 ms from pulse onset) subtracted from depolarization at the peak. In gray: control neurons, in black: deprived neurons. Dashed line separates PS from RS neurons: PS neurons always had OR drop values >1.7 mV. *D*: time T to overall AHP peak (evoked by APs, measured before TTX perfusion) vs. late OR voltage drop (in absence of APs, after TTX perfusion) for PS ($n = 6$) and RS ($n = 2$) neurons. Large late AHPs and late ORs always appeared together, and data fell into 2 distinct groups depending on scored spiking behavior. Each symbol denotes an individual experiment. *E*: late OR voltage drop vs. spike ratio R for PS ($n = 6$) and RS ($n = 2$) neurons. Neurons fell into 2 groups also determined by scored spiking behavior. Key as for *D*.

Maturation of spiking patterns was significantly delayed by whisker deprivation (Fig. 1*C*; 3-way table, log-linear independence test, $P < 0.004$). Deprivation decreased the fraction of RS cells at ages PND 14 and 17 (Fig. 1*C*); its effect became significant when comparing across ages.

In layer 4, 100% of cells showed RS behavior at age PND 14 both in control and deprived conditions ($n = 6$ of 6 and 4 of 4, respectively; Fig. 1*C*). Therefore at this age, layer 4 spiny stellate spiking behavior was already as for mature spiny stellate neurons. This is consistent with the earlier critical period for response plasticity observed in this layer (Fox 1992).

We conducted further analysis of spiking behavior through the spike ratio R. Stimuli had 500-ms duration, and R was equal to the ratio of the numbers of spikes fired during the second and first 100 ms after stimulus onset (see METHODS). R correlated very well with spiking behavior as scored by the experimenter: RS neurons had a significantly higher R value than PS neurons (Fig. 1*D*; Mann-Whitney U test, $P < 0.0001$). Consistent with this, R values increased during development (Fig. 1*E*). Whisker deprivation also decreased R in a manner compatible with a deprivation-induced delay in maturation (Fig. 1*E*). Both age and deprivation had a statistically significant effect on R values (2-way ANOVA, after log-ANOVA test for homogeneity of variances; age, $P < 0.02$; deprivation, $P < 0.05$; sample sizes: $n = 23$ for PND 12 control, $n = 21$ for PND 12 deprived, $n = 35$ for PND 14 control, $n = 32$ for PND 14 deprived, $n = 17$ for PND 17 control, $n = 22$ for PND 17 deprived). R values of PND 14 spiny stellate neurons were close to 1 and were not

significantly different for control and deprived neurons (control, $n = 7$; deprived, $n = 5$; Fig. 1*E*).

Consistent with previous studies, we found that the amount of SFA of a cell and therefore its spiking pattern could vary during the course of experiments (Borde et al. 1995, 2000; Lorenzon and Foehring 1995; Zhang et al. 1995). Soon after breaking into whole cell configuration (sometimes as early as 2-3 min after break-in), RS cells often displayed increased adaptation, switching eventually (~5-10 min) to PS behavior. For younger animals, the great majority of RS neurons underwent this change. These cells were healthy by all electrophysiological criteria including stability of resting membrane potential, input impedance, and spike parameters, and all experiments were performed using internal solution based on K^+-methylsulfonate, which provides the most stable recording conditions (Velumian et al. 1997; Zhang et al. 1994). Furthermore, we excluded Ca^{2+} buffers from the pipette solution, so the change was not due to the effects of BAPTA or other buffers (Lancaster and Batchelor 2000; Lorenzon and Foehring 1995; Schwindt et al. 1992; Zhang et al. 1995). Finally, stability of spike patterns did not appear to depend on the history of activity: neurons switched spiking behavior even if kept silent during the first few minutes of a recording. The mechanisms determining regular or phasic spiking could therefore undergo rapid changes. Classifying RS cells into "regular" and "switching" categories according to whether they did or did not switch spiking patterns under these conditions revealed a sig-

nificant difference in the distribution of categories between control and deprived groups (Fig. 1F; G-test, $P < 0.025$).

Membrane potential, passive properties, and spike properties

We measured basic intrinsic properties (resting membrane potential, input impedance, membrane time constant, spike height and width, absolute and relative spiking threshold: Tables 1 and 2). Developmental changes in layer 2/3 cells included a decrease in input impedance, a small hyperpolarization in resting potential, a faster membrane time constant, and larger and faster action potentials with a lower threshold. These changes agreed with those previously found in other cortical neurons (Kasper et al. 1994). We found no differences in any of these properties between cells from control and deprived animals at any age.

Layer 4 cells at age PND 14 showed properties similar to layer 2/3 cells of the same age with the exception of input impedance, which was significantly higher for spiny stellates (layer 4: 302 ± 36 MΩ, layer 2/3: 213 ± 14 MΩ; *t*-test, $P < 0.05$), as expected based on their small size.

Current-frequency relationships

We next evaluated the relationship between stimulation current intensity and instantaneous spiking frequency (calculated for the 1st 2 APs fired; Fig. 2A). This provided a measure of neuronal excitability during the early part of responses, before the onset of SFA. Current-frequency (*I-f*) curves averaged over all PND 14 cells are plotted in Fig. 2B, showing the different responses of layer 4 and 2/3 neurons. Current-frequency relationships were not experience-dependent at any age. Layer 2/3 neurons were responsive at intensities as low as layer 4 spiny stellate cells, even though these have higher input impedances (Table 1) by virtue of their morphology.

We further characterized each cell's *I-f* curve using its maximum slope (f'_{max}) and the current intensity at which the maximum slope was reached [$I(f'_{max})$]. By definition, $I(f'_{max})$ is the current at which a cell is maximally responsive, i.e., maximally able to modulate its spike frequency in response to changes in input. More excitable cells are maximally responsive at smaller inputs [smaller $I(f'_{max})$] than less excitable cells. Maximum slope, f'_{max}, was not affected by deprivation (Fig. 2C). Because the data did not vary significantly across control and deprived conditions for any of the age groups (*t*-test for means, *F* test for variances), we could pool data from control and deprived conditions for each age. This revealed a nonsignificant developmental increase in f'_{max} for layer 2/3 cells at

PND 17. The f'_{max} of layer 4 cells and layer 2/3 cells differed significantly at PND 14 (*t*-test, $P < 0.0001$): this is explained simply by the ability of spiny stellate cells to fire at higher frequencies.

Deprivation had no effect on the current at which the maximum slope was reached, $I(f'_{max};$ Fig. 2D). As for effects of development, although $I(f'_{max})$ did not change from PND 12 to 14, it decreased significantly from PND 12 to 17 (Fig. 2D; *t*-test, $P < 0.05$; data pooled across conditions after satisfying the *F* test for homogeneity). The decrease in $I(f'_{max})$ implies that older cells are more responsive to small inputs, in spite of their smaller input impedance (Table 1).

Because a cell's $I(f'_{max})$ is affected by its passive properties (lower impedance implies that a higher current is necessary to achieve a given depolarization), we scaled $I(f'_{max})$ by the cells' input resistances measured at resting potential. The resulting number *V** is not a measure of true depolarization or excitation in response to realistic inputs, but allows comparison across groups (Fig. 2E). *V** was again not affected by deprivation. Although *V** did not change in layer 2/3 neurons from PND 12 to 14, it decreased significantly from PND 14 to 17 (*t*-test, $P < 0.01$ from either of the earlier ages to PND 17; data pooled across conditions after satisfying the *F* test for homogeneity). Therefore maturation of membrane properties shifts the *I-f* curve to the left (i.e., cells are responsive to smaller net inputs). Layer 2/3 excitability as measured by *V** was higher than for layer 4 (Fig. 2E), allowing cells to be sensitive to weaker synaptic input (Feldmeyer et al. 2002).

Spiking behavior and slow AHP

We next focused our analysis on neuronal properties that correlated with spiking behavior. Spike frequency adaptation appeared highly correlated with the magnitude of a slow AHP. However, prominent fast AHPs could be present in neurons regardless of age or spike frequency adaptation behavior. We therefore quantified AHPs using a standardized protocol that consisted of stimulating cells with 10 APs fired at 100 Hz (Fig. 3A). The overall AHP varied in magnitude, time to peak, and duration, indicating the varying contribution of a slow AHP with a time to peak of several hundred (~500) ms and a time course of 1-1.5 s (Fig. 3A).

Grouping neurons by their spiking behavior (RS and PS groups; only PND 17 cells with stable spiking behavior were included in this analysis) revealed variations in slow AHP across spiking type. RS and PS cells did not differ significantly in the magnitude of the fast AHP peak. However, slow AHPs (time to peak: ~500 ms) were significantly more prominent in

TABLE 1. *Passive properties*

| | Layer 2/3 | | | | | | Layer 4 | |
| | PND 12 | | PND 14 | | PND 17 | | PND 14 | |
	Control	Deprived	Control	Deprived	Control	Deprived	Control	Deprived
n	5	9	12	10	8	6	6	4
V_m, mV	-71.4 ± 3.7	-68.2 ± 1.5	-70.2 ± 1.6	-72.9 ± 1.8	-72.8 ± 1.4	-72.0 ± 1.7	-68.3 ± 2.9	-72.8 ± 1.6
τ_c, ms	21.8 ± 2.6	23.6 ± 1.7	18.1 ± 1.3	20.4 ± 1.4	16.3 ± 1.1	16.6 ± 1.8	19.8 ± 1.9	14.9 ± 1.1
R_{in}, MΩ	255 ± 31	246 ± 22	192 ± 13	238 ± 25	171 ± 16	168 ± 18	317 ± 54	279 ± 46

Passive properties grouped by layer, age and condition. V_m; resting membrane potential; τ_c, membrane time constant; R_{in}: input resistance. Values show means $\pm$ SE.

TABLE 2. *Action potential properties*

	Layer 2/3						Layer 4	
	PND 12		PND 14		PND 17		PND 14	
	Control	Deprived	Control	Deprived	Control	Deprived	Control	Deprived
n	6	8	12	10	7	6	6	4
H, mV	69.7 ± 4.1	69.3 ± 3.2	78.3 ± 3.1	72.6 ± 2.1	80.6 ± 2.7	85.8 ± 3.5	80.7 ± 2.6	75.8 ± 1.4
W, ms	1.10 ± 0.09	1.23 ± 0.05	1.15 ± 0.09	0.98 ± 0.05	0.99 ± 0.05	0.98 ± 0.05	1.03 ± .08	0.88 ± 0.03
V_{thr}, mV	−34.5 ± 2.6	−34.4 ± 0.81	−36.2 ± 1.3	−34.9 ± 1.5	−36.4 ± 2.4	−36.7 ± 1.5	−37.2 ± 1.5	−38.8 ± 0.75
V_{rel}, mV	33.8 ± 1.2	32.6 ± 1.3	33.7 ± 1.6	37.9 ± 1.6	35.3 ± 1.9	33.3 ± 2.5	32.2 ± 1.4	35.0 ± 1.8

Action potential properties grouped by layer, age, and condition. H, height from inflection point to peak; W, full width at half-height; V_{thr}, threshold potential; V_{rel}, threshold potential relative to rest. Values show means ± SE.

PS neurons (Fig. 3A), where they dominated the overall AHP, as reflected in the time T elapsed from stimulation onset to overall AHP peak (Fig. 3, B and C). When T was plotted against the spike ratio R, data points clustered into groups corresponding to the PS and RS categories (Fig. 3B). In PS neurons at PND 17 (Fig. 3C) $T = 291 ± 27$ ms ($n = 5$) while in RS neurons $T = 159 ± 8$ ms ($n = 6$). This difference was significant (t-test, $P < 0.01$). Further, AHP amplitudes measured 400 ms after stimulation offset (a time when the slow AHP is the major contributor to the AHP waveform; Fig. 3D) were (PS neurons, $n = 5$) $V_{AHP, 400} = 7.1 ± 1.1$ mV, (RS neurons, $n = 6$) $V_{AHP, 400} = 3.6 ± 1.0$ mV. These values were significantly different (t-test, $P < 0.05$). In a group of neurons that switched from RS to PS behavior during recording (see preceding text), we tracked the evolution of the slow AHP's magnitude as the cells switched behavior. Slow AHP magnitude grew during the experiment in 14 of 16 neurons monitored. In $n = 3$ switching neurons, trials using AP trains (to measure the AHP) were interleaved with trials using single depolarizing pulses (to determine the spike ratio R): AHP magnitude measured at 7-12 min after break-in was $92 ± 42\%$ larger than measured at 0-5 min after break-in. This change in the AHP occurred while the neurons' spiking was becoming more phasic: the relative decrease in R over the same period was $78 ± 22\%$. Thus spiking behavior was correlated with slow AHP magnitude.

We next grouped PND 17 neurons by control or deprived condition irrespective of spiking behavior. Deprivation had significant effects on the slow AHP (Fig. 3, E and F): the AHP magnitude measured 400 ms after stimulation offset (Fig. 3F) was significantly increased by deprivation (control neurons: $V_{AHP, 400} = 3.2 ± 0.5$ mV, $n = 17$; deprived neurons: $V_{AHP, 400} = 5.0 ± 0.7$ mV; t-test, $P < 0.05$). However, the time T to overall peak (Fig. 3E) did not differ significantly across groups (control neurons: $T = 248 ± 25$ ms, $n = 17$; deprived neurons: $T = 255 ± 16$ ms, $n = 17$): because RS and PS neuronal types were distributed across control and deprived conditions, differences in AHP parameters were diluted. Therefore the amplitude of the slow AHP correlates with spiking behavior and is regulated by sensory experience.

Spiking behavior and outward rectification

Comparison of PS versus RS patterns further revealed that PS behavior was correlated with a characteristic response waveform that combined an earlier, slow depolarization peak with a later, less depolarized plateau phase (compare voltage traces in Fig. 1, B and A). This behavior was present also during subthreshold responses (Fig. 4A). In PS neurons, APs were generated only during the early depolarization peak. In contrast, RS neurons never showed this characteristic behavior (Fig. 4B). We thus looked for a possible relationship to the slow AHP. We hypothesized that the end of the peak depolarization phase of PS responses might be the onset of a slow hyperpolarization, causing a late increase in outward rectification (OR). Because the putative OR occurred also during subthreshold responses, we characterized the phenomenon by depolarizing neurons in the presence of TTX (1 μM). Responses were measured on depolarization with 500-ms duration current pulses (Fig. 4, A and B). Measurements were taken at two times: the time of peak response, and late in a pulse (450-500 ms), when depolarization had reached steady state (Fig. 4, A and B). The difference between response magnitudes at these times was used as a measure of OR (Fig. 4C; 500-pA current pulses).

As expected, PS but not RS neurons had a substantial amount of OR that was maintained even after TTX had blocked spiking (PS, Fig. 4A; RS, Fig. 4B; collected data, Fig. 4C). We further quantified the amount of OR using I-V curves for depolarization starting from identical resting potentials. I-V curves were measured early in a pulse (at peak response, see Fig. 4A) and at steady state, late in a pulse (450-500 ms after pulse onset; Fig. 4A). We took the ratio of the I-V slope at rest (i.e., the input resistance) to the I-V slope at strongly depolarizing currents (data not shown). If a significant amount of late OR was present, this ratio was larger for I-V curves at steady state than for I-V curves at peak response. Dividing the late ratio by the peak ratio thus gave an index of late OR. PS cells had a significantly larger late OR index than RS cells (t-test, $P < 0.02$; $n = 6$ and $n = 2$, respectively).

In addition, the late OR correlated strongly with the slow AHP because neurons with a large slow AHP component (as measured by a long time to peak AHP) also had large late OR voltage drops (Fig. 4D). Plotting the OR voltage drop against the spike ratio R showed clustering corresponding to the RS and PS categories, showing that both the slow AHP and the OR covaried with spiking behavior (Fig. 4E). This correlation between the slow AHP and the delayed OR suggested the possibility that they might share an underlying slow hyperpolarizing current that would contribute to terminating spiking.

Regulation of adaptation and spiking behavior

Delayed hyperpolarization mechanisms clearly could play an important role in determining spiking patterns. One candidate mechanism for PS behavior was the comparatively slow and low-threshold "I_D" K^+ current (Locke and Nerbonne 1997). However, we found that blocking I_D with 4-aminopyridine (50 μM; after TTX application) (Fig. 4A, *right*; repeated in $n = 2$ experiments) did not reduce OR, indicating that I_D did not play a significant role in the determination of PS or RS behavior.

Changes in slow AHPs (Schwindt et al. 1988a,b, 1992) have been shown to be involved in spiking behavior maturation in cortical pyramidal cells (Lorenzon and Foehring 1993). We evaluated whether differences in slow AHPs were involved in shaping the depolarization waveforms distinguishing PS cells from RS cells, and whether these differences were dependent on Ca^{2+} influx. To do so, we examined whether PS patterns depended on calcium entry by using $CdCl_2$ (50 μM) to block influx through Ca^{2+} channels. In all cells tested ($n = 5$), $CdCl_2$ induced RS behavior (Fig. 5A) and reduced the size of the slow AHP ($V_{AHP, 400}$ reduced to 0.29 ± 0.09 of baseline value; Fig. 5, *B* and *C*). Both the reduction in the slow AHP and the increase in spike ratio R induced by $CdCl_2$ were significant (paired *t*-test; AHP: $P < 0.025$; R: $P < 0.02$; Fig. 5C): PS behavior and the slow AHP were jointly dependent on Ca^{2+}.

We attempted to disentangle the origin of the developmental and experience-dependent regulation of spiking behavior and AHPs. Maturational changes could be due either to changes in

the hyperpolarizing currents themselves or to changes upstream of those currents in the mechanisms regulating their strength: for instance, in Ca^{2+} entry and/or in the driving force due to depolarization. We ruled out Na^+-mediated changes in depolarization based on two criteria: first, TTX application had no effect on the late OR characteristic of PS cells (Fig. 4), excluding participation of TTX-sensitive Na^+ currents in determining this behavior. Second, PS behavior was eliminated by $CdCl_2$, excluding participation of TTX-insensitive, persistent Na^+ currents because these are not sensitive to $CdCl_2$ application (Brumberg et al. 2000; Crill 1996).

We next tested for a contribution of changes in Ca^{2+}-mediated depolarizations or in Ca^{2+} entry to the developmental process leading from PS to RS behavior. First, we tested for participation of T-type Ca^{2+} currents in the enhanced slow AHP and late OR characteristic of PS behavior by raising the holding membrane potential to between -55 and -50 mV with a positive current, enough to inactivate T-type currents (Hille 2001). Depolarized holding potentials did not change spiking waveforms from PS- to RS-like (Fig. 5D) or reduce slow AHPs (Fig. 5, *D* and *E*): instead, raising the holding voltage linearly increased the magnitude of the slow AHP (Fig. 5E; repeated $n = 5$ times), consistent with a dependence only on the reversal potential of K^+. This ruled out a significant effect of T-type Ca^{2+} influx on spiking behavior and the slow AHP.

We searched for developmental changes in Ca^{2+} fluxes and handling. $[Ca^{2+}]$ imaging experiments were performed at PND
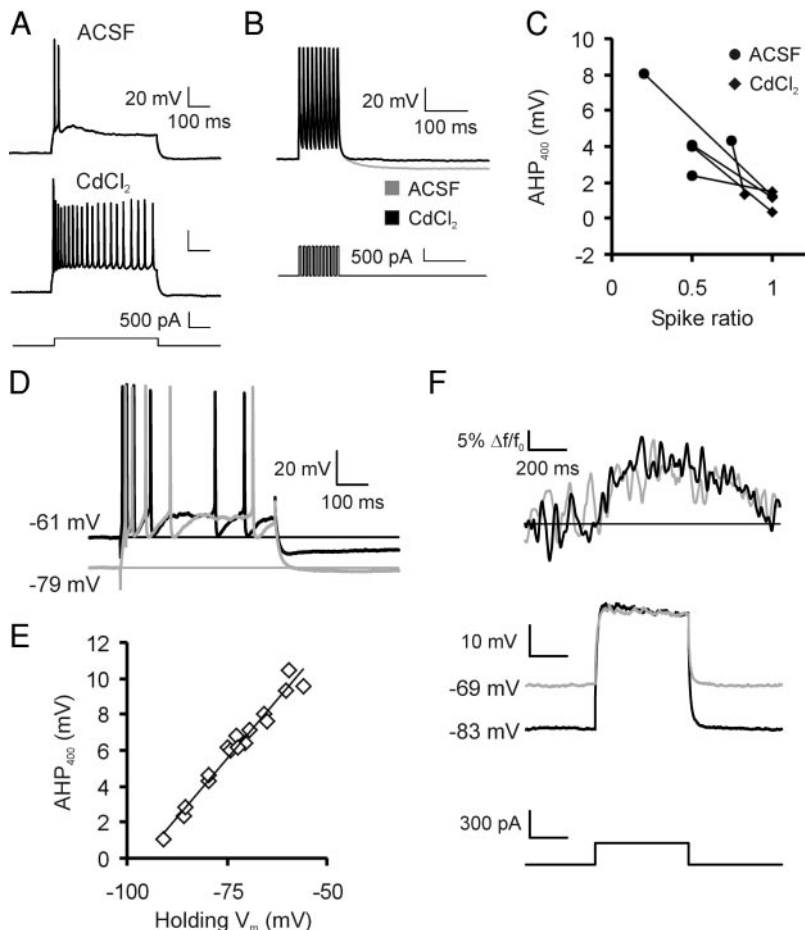

FIG. 5. Spiking behavior and the slow AHP are Ca^{2+}-influx dependent. *A*: traces from a PS cell showing responses in drug-free ACSF (*top*) and in 50 μM $CdCl_2$ (*middle*); both responses are to 250-pA depolarizing current pulses (*bottom*). PS behavior became RS after $CdCl_2$ perfusion. *B*: decrease in slow AHP after $CdCl_2$ perfusion. AHP recorded using the standard protocol (*bottom*; Fig. 3). Superimposed voltage traces (*top*) show responses to same AP train before and after $CdCl_2$ application. *C*: slow AHP decreased and spike ratio R increased in all $n = 5$ $CdCl_2$ experiments. Each line connects pre- and post-$CdCl_2$ measurements within an experiment. Circles: before $CdCl_2$ application, diamonds: after $CdCl_2$ application. *D*: depolarized response spike waveforms do not depend on holding voltage, but slow AHP increases in magnitude with more depolarized holding voltage. In gray: recording from resting potential (-79 mV), in black: recording from depolarized holding potential (-61 mV) at positive current. *E*: dependence of slow AHP on holding potential is linear, with an apparent reversal potential close to K^+. Points are taken from 1 experiment, but result was repeated $n = 5$ times. Line is linear fit to data. *F*: subthreshold $[Ca^{2+}]$ transients. *Bottom*: 240-pA depolarizing current pulse, which was subthreshold for the neuron depicted. *Middle*: voltage responses with no holding current and with depolarizing holding current (respectively, black, -83 mV; and gray, -69 mV). *Top*: corresponding fluorescence increases ($\Delta f/f_0$) in the proximal apical dendrite. Thin line shows baseline fluorescence, f_0. Fluorescence increases were very slow and did not depend on holding voltage.

12-17, using the BAPTA-based dye OGB-1 (see METHODS). Because BAPTA alters Ca^{2+} chelation and interferes with intrinsic Ca^{2+} buffers including Ca^{2+}-activated K^+ channels (Lancaster and Batchelor 2000), we expected dye perfusion to make immature neurons highly susceptible to switching their spiking behavior. Indeed, moderate concentrations of OGB-1 BAPTA (50-100 μM) always induced switching to PS behavior and enhanced the slow AHP ($n = 16$; data not shown), consistent with previous reports (Borde et al. 1995; Jahromi et al. 1999; Lorenzon and Foehring 1995; Schwindt et al. 1992; Velumian and Carlen 1999; Zhang et al. 1995) and with the relationship between spiking behavior and the Ca^{2+}-dependent slow AHP (Figs. 3 and 5). For this reason, we did not divide the data into PS and RS cell types. Instead, we classified our [Ca^{2+}] recordings by age group (Table 3) with more immature neurons corresponding to more phasic responses. We found no significant developmental changes in AP-evoked (high-threshold) [Ca^{2+}] increases or in Ca^{2+} buffer capacity in the proximal apical dendrite (Table 3).

However, during imaging experiments, we often observed small [Ca^{2+}] transients under depolarizations that remained subthreshold for AP generation (Fig. 5F). These transients were always in neurons with PS behavior and prominent slow AHPs. The switch to more phasic spiking that occurred in the majority of imaging experiments (see preceding text) together with an increase in slow AHP were always accompanied by the appearance of subthreshold [Ca^{2+}] transients. Subthreshold [Ca^{2+}] transients were slow, with a rise time of tens of milliseconds building to a peak of several hundred milliseconds, indicating that they were due to a noninactivating source. This ruled out participation of T-, N-, P-, Q-, or R-type channels (Hille 2001). T-type channels were, in addition, ruled out because, similarly to the slow AHP (Fig. 5E), subthreshold [Ca^{2+}] transients did not decrease at elevated holding potentials (Fig. 5F). L-type channels are likely involved because application of nimodipine (10 μM) appeared to eliminate subthreshold Ca^{2+} entry ($n = 3$; data not shown) and reduced slow AHP magnitude in PS neurons (by $35.5 \pm 1.0\%$, $n = 4$; data not shown). Facilitated entry through L-type channels is consistent with evidence showing that L-type channels in pyramidal neurons can contribute to Ca^{2+} entry at low voltages (Avery and Johnston 1996; Magee et al. 1996) and undergo voltage-dependent facilitation (Dolphin 1996). Facilitation can occur even with moderate depolarizing voltages (Svirskis and Hounsgaard 1997). Short AP trains can generate prolonged enhancement of D class L-type channel activation at membrane

potentials negative to -50 mV (Cloues et al. 1997). In hippocampal pyramidal neurons, this delayed facilitation of L-type channels can directly evoke slow AHP waveforms (Bowden et al. 2001), and L-type activation underlies potentiation of the slow AHP during experiments (Borde et al. 2000). Consistent with this, in our experiments nimodipine had negligible effects on AHP magnitude in neurons that remained RS (data not shown). However, nimodipine did not systematically switch spiking behavior back from PS to RS or significantly increase R ($44 \pm 29\%$, $n = 3$).

Inward rectification and sag potentials

Other intrinsic properties measured included fast and slow inward rectification under hyperpolarization. Under hyperpolarizing stimulation, cortical pyramidal cells display fast inward rectification dependent on a K^+ current (Hille 2001) as well as a depolarizing voltage "sag" due to activation of I_h, a slowly activating, [Ca^{2+}]-regulated nonspecific cation current with important effects on excitability (Luthi and McCormick 1998; Pape 1996). I_h plays an important role in the activation and maintenance of spontaneous rhythmic patterns in the CNS and elsewhere (Luthi and McCormick 1998; McCormick and Pape 1990).

Sag depolarization decreased with age while early inward rectification grew. PND 12 and 14 neurons had significantly larger sags than PND 17 cells (data not shown; t-test significance levels: PND 12 vs. 17, $P < 0.0001$; PND 14 vs. 17, $P < 0.001$) and significantly smaller rectification (t-test; PND 12 vs. 17, $P < 0.005$; PND 14 vs. 17, $P < 0.01$). This developmental effect on sag depolarization is in the same direction as has been observed in layer 1 neocortical cells (Zhou and Hablitz 1996), but in the opposite direction to changes observed in other systems (Reece and Schwartzkroin 1991; Viana et al. 1994). There was no effect of sensory deprivation or of cell layer location.

DISCUSSION

We probed intrinsic cellular response properties as a function of developmental age and sensory experience. Maturation of the spiking behavior of excitatory layer 2/3 BC neurons coincides in time with the closing of the critical period for sensory map plasticity. Changes in spiking properties are related to changes in a slow AHP.

Layer 2/3 responses change from being mostly phasic to being mostly regular during the period PND 12-17 in synchrony with intracortical synaptogenesis (Micheva and Beaulieu 1996) and with extensive experience-dependent synaptic (Lendvai et al. 2000) and dendritic (Maravall et al. 2004) rearrangement. This period immediately follows the beginning of active whisker exploration (Welker 1964). In contrast, layer 4 spiny stellate cells, with earlier critical periods for synaptic input plasticity (before PND 7) (Crair and Malenka 1995; Feldman et al. 1998) and subthreshold receptive fields (Stern et al. 2001), have mature response properties by PND 14. Maturation of layer 2/3 spiking behavior and therefore of neuronal responsiveness is delayed by sensory deprivation (Fig. 1C).

Because more mature RS neurons could sustain spiking throughout a 500-ms stimulus pulse, their excitability mea-

TABLE 3. *Calcium regulation*

	PND 12	PND 14	PND 17
[Ca^{2+}]$_0$ (nM)	37–49	28–37	25–31
n	5	6	5
Δ[Ca^{2+}] (nM)	299–455	306–373	322–347
n	3	4	5
κ	36–50	35–60	51–55
n	3	5	4
Δ[Ca^{2+}]$_{tot}$ (μM)	14.3–16.2	11.9–12.0	15.8–16.1
n	3	4	4

Regulation of calcium concentration in the proximal apical dendrite, grouped by age. [Ca^{2+}]$_0$, resting [Ca^{2+}]$_0$; Δ[Ca^{2+}]; rise in free [Ca^{2+}] evoked by a single AP; κ, calcium buffering capacity; Δ[Ca^{2+}]$_{tot}$, rise in total [Ca^{2+}] evoked by a single AP. Values show range.

sured in terms of number of APs fired was greater than that of PS neurons. RS neurons can respond to stronger depolarization with an increasing number of spikes. In contrast, because PS neurons stop spiking before stimulation ends, the overall number of spikes generated by these neurons is not highly sensitive to increases in depolarization. PS responses of immature cells resemble bursts and could help promote synchrony of cortical responses. Correlated activity in the immature cortex is well known (Garaschuk et al. 2000; Katz and Shatz 1996; Mao et al. 2001; Schwartz et al. 1998) and could enhance correlation-based synaptic plasticity (Katz and Shatz 1996).

Our data suggest that layer 2/3 PS neurons are an immature form of RS neurons (Montoro et al. 1988) rather than a distinct category of intrinsically bursting neurons (Zhu and Connors 1999) present only in the developing animal (Metherate and Aramakis 1999). This idea is supported by the finding that the short spike sequences fired by PS cells were not stereotyped AP bursts (Nowak et al. 2003), according to several criteria. First, minimal spike frequencies varied across PS cells as much as they did over RS cells. Second, spike frequencies over the first one or two interspike intervals were as tunable by stimulus magnitude in PS cells as they were in RS cells. Third, PS and RS cells did not have noticeable differences in spike threshold or in the ratio between thresholds for single spikes and for spike pairs. Neurons showing RS and PS behavior differed only in the mechanisms specifically responsible for determining SFA.

What mechanisms participate in the changes observed in spiking behavior? A variety of ionic currents are capable of contributing to PS or RS behaviors and their developmental regulation (see e.g., Amitai and Connors 1995). In several classes of neurons (Wang et al. 1997), phasic spiking can be promoted by slow recovery from inactivation of Na^+ currents, which is a mark of immaturity. For instance, immature retinal ganglion cells are usually rapidly adapting and often show single-spike discharges. Na^+ currents of single-spike neurons have significantly slower speeds of recovery from inactivation than those of rapidly adapting cells, which in turn recover significantly slower than Na^+ currents of RS cells. These differences are due to a developmental change in Na^+ channel subtype expression at the initial axonal segment of ganglion cells (G. Matthews, personal communication) like that in optic nerve nodes of Ranvier (Boiko et al. 2001). At the youngest age recorded in the present study (PND 12), we found a subgroup of PS neurons that had difficulty firing more than one spike in response to depolarization, suggesting slow recovery from inactivation of Na^+ channels. However, we found that PS neurons differed from RS neurons in that they always showed a large late OR. This OR was not abolished by TTX (Fig. 4) and therefore could not be explained by differences in expression of inactivating Na^+ channels. Another candidate mechanism for promoting PS behavior is the I_D K^+ current (Locke and Nerbonne 1997). Our experiments ruled out a role of I_D in shaping PS spiking behavior: blocking I_D did not induce reductions in the OR that would make cells more RS-like (Fig. 4).

Our results were consistent with a role of a slow AHP (Schwindt et al. 1988a, b, 1992) in maturation of spiking behavior (Lorenzon and Foehring 1993) (Fig. 3). Both spiking behavior and the slow AHP were modified by $CdCl_2$, implying

that they depended on Ca^{2+} influx (Fig. 5). Changes in AHP size and in SFA could also be induced by BAPTA perfusion and could occur rapidly, on the time scale of a whole cell experiment (within 10–20 min). This suggested that modulation of Ca^{2+} entry and handling was a more likely reason for the developmental changes in the AHP than alterations in the expression of the AHP channels themselves. Our imaging experiments did not detect any developmental changes in either AP-evoked $[Ca^{2+}]$ increases or in Ca^{2+} buffer capacity measured in the proximal apical dendrite (Table 3) but did reveal the presence of slow subthreshold $[Ca^{2+}]$ transients in PS but not RS neurons (Fig. 5F). This supports the possibility of developmental adjustments in Ca^{2+} entry mechanisms. Previous studies (Lorenzon and Foehring 1995; Schwindt et al. 1992) have suggested that modifications in the dominant sources of Ca^{2+} influx are responsible for changes in slow AHP magnitude and spiking behavior. Slow Ca^{2+}-dependent AHP currents are a target of experience- and training-dependent plasticity in several brain regions (Coulter et al. 1989; Disterhoft et al. 1986, 1988; Saar and Barkai 2003; Schreurs et al. 1998). Increases in intrinsic excitability due to a reduction in AHP may have a permissive function in circuit plasticity and memory (Moyer et al. 1996; Thompson et al. 1996; Zhang and Linden 2003).

Layer 2/3 subthreshold sensory maps are affected by deprivation started around PND 9-12 but not later (Stern et al. 2001). Layer 4–layer 2/3 synaptic plasticity can still be evoked at later ages (Allen et al. 2003; Feldman 2000). Additional plasticity mechanisms (Maravall et al. 2004) are required to explain the critical period for layer 2/3 subthreshold sensory maps.

DISCLOSURES

Present address of E. A. Stern: Dept. of Neurology, Massachusetts General Hospital, 144 16th St., Charlestown, MA 02129.

REFERENCES

Aizenman CD, Akerman CJ, Jensen KR, and Cline HT. Visually driven regulation of intrinsic neuronal excitability improves stimulus detection in vivo. *Neuron* 39: 831–842, 2003.

Aizenman CD and Linden DJ. Rapid, synaptically driven increases in the intrinsic excitability of cerebellar deep nuclei neurons. *Nat Neurosci* 3: 109–111, 2000.

Allen CB, Celikel T, and Feldman DE. Long-term depression induced by sensory deprivation during cortical map plasticity in vivo. *Nat Neurosci* 6: 291–299, 2003.

Amitai Y and Connors BW. Intrinsic physiology and morphology of single neurons in neocortex. In: *The Barrel Cortex of Rodents*, edited by Jones EG and Diamond IT. New York: Plenum, 1995, p. 299-324.

Armano S, Rossi P, Taglietti V, and D'Angelo E. Long-term potentiation of intrinsic excitability at the mossy fiber-granule cell synapse of rat cerebellum. *J Neurosci* 20: 5208–5216, 2000.

Armstrong-James M, Callahan CA, and Friedman MA. Thalamo-cortical processing of vibrissal information in the rat. I. Intracortical origins of

surround but not center-receptive fields of layer IV neurones in the rat S1 barrel field cortex. *J Comp Neurol* 303: 193–210, 1991.

Armstrong-James M, Diamond ME, and Ebner FF. An innocuous bias in whisker use in adult rats modifies receptive fields of barrel cortex neurons. *J Neurosci* 14: 6978–6991, 1994.

Armstrong-James M and Fox K. Spatiotemporal convergence and divergence in the rat S1 "barrel" cortex. *J Comp Neurol* 263: 265–281, 1987.

Armstrong-James M, Fox K, and Das-Gupta A. Flow of excitation within rat barrel cortex on striking a single vibrissa. *J Neurosci* 68: 1345–1354, 1992.

Avery RB and Johnston D. Multiple channel types contribute to the low-voltage-activated calcium current in hippocampal CA3 pyramidal neurons. *J Neurosci* 16: 5567–5582, 1996.

Boiko T, Rasband MN, Levinson SR, Caldwell JH, Mandel G, Trimmer JS, and Matthews G. Compact myelin dictates the differential targeting of two sodium channel isoforms in the same axon. *Neuron* 30: 91–104, 2001.

Borde M, Bonansco C, Fernandez de Sevilla D, Le Ray D, and Buno W. Voltage-clamp analysis of the potentiation of the slow Ca-activated K current in hippocampal pyramidal neurons. *Hippocampus* 10: 198–206, 2000.

Borde M, Cazalets JR, and Buno W. Activity-dependent response depression in rat hippocampal CA1 pyramidal neurons in vitro. *J Neurophysiol* 74: 1714–1729, 1995.

Bowden SEH, Fletcher S, Loane DJ, and Marrion NV. Somatic colocalization of rat SK1 and D class (Ca$_v$ 1.3) L-type calcium channels in rat CA1 hippocampal pyramidal neurons. *J Neurosci* 21: RC175 (1–6), 2001.

Brumberg JC, Nowak LG, and McCormick DA. Ionic mechanisms underlying repetitive high-frequency burst firing in supragranular cortical neurons. *J Neurosci* 20: 4829–4843, 2000.

Cloues RK, Tavalin SJ, and Marrion NV. β-adrenergic stimulation selectively inhibits long-lasting L-type calcium channel facilitation in hippocampal pyramidal neurons. *J Neurosci* 17: 6493–6503, 1997.

Connors BW and Gutnick MJ. Intrinsic firing patterns of diverse neocortical neurons. *Trends Neurosci* 13: 99–104, 1990.

Coulter DA, Lo Turco JJ, Kubota M, Disterhoft JF, Moore JW, and Alkon DL. Classical conditioning reduces amplitude and duration of calcium-dependent afterhyperpolarization in rabbit hippocampal pyramidal cells. *J Neurophysiol* 61: 971–981, 1989.

Crair MC and Malenka RC. A critical period for long-term potentiation at thalamocortical synapses. *Nature* 375: 325–328, 1995.

Crill WE. Persistent sodium current in mammalian central neurons. *Annu Rev Physiol* 58: 349–362, 1996.

Daoudal G, Hanada Y, and Debanne D. Bidirectional plasticity of excitatory postsynaptic potential (EPSP)-spike coupling in CA1 hippocampal pyramidal neurons. *Proc Natl Acad Sci USA* 99: 14512–14517, 2002.

Davis GW and Bezprozvanny I. Maintaining the stability of neural function: a homeostatic hypothesis. *Annu Rev Physiol* 63: 847–869, 2001.

De Felipe J, Marco P, Fairen A, and Jones EG. Inhibitory synaptogenesis in mouse somatosensory cortex. *Cereb Cortex* 7: 619–634, 1997.

Dégenètais E, Thierry A-M, Glowinski J, and Gioanni Y. Electrophysiological properties of pyramidal neurons in the rat prefrontal cortex: an in vivo intracellular recording study. *Cereb Cortex* 12: 1–16, 2002.

Desai NS, Rutherford LC, and Turrigiano GG. Plasticity in the intrinsic excitability of cortical pyramidal neurons. *Nat Neurosci* 2: 515–520, 1999.

Diamond ME, Huang W, and Ebner FF. Laminar comparison of somatosensory cortical plasticity. *Science* 265: 1885–1888, 1994.

Disterhoft JF, Coulter DA, and Alkon DL. Conditioning-specific membrane changes of rabbit hippocampal neurons measured in vitro. *Proc Natl Acad Sci USA* 83: 2733–2737, 1986.

Disterhoft JF, Golden DT, Read HL, Coulter DA, and Alkon DL. AHP reductions in rabbit hippocampal neurons during conditioning correlate with acquisition of the learned response. *Brain Res* 462: 118–125, 1988.

Dolphin AC. Facilitation of Ca^{2+} current in excitable cells. *Trends Neurosci* 19: 35–43, 1996.

Feldman DE, Nicoll RA, Malenka RC, and Isaac JT. Long-term depression at thalamocortical synapses in developing rat somatosensory cortex. *Neuron* 21: 347–357, 1998.

Feldman DE. Timing-based LTP and LTD at vertical inputs to layer II/III pyramidal cells in rat barrel cortex. *Neuron* 27: 45–56, 2000.

Feldmeyer D, Lubke J, Silver RA, and Sakmann B. Synaptic connections between layer 4 spiny neurone-layer 2/3 pyramidal cell pairs in juvenile rat barrel cortex: physiology and anatomy of interlaminar signalling within a cortical column. *J Physiol* 538: 803–822, 2002.

Finnerty GT, Roberts LS, and Connors BW. Sensory experience modifies the short-term dynamics of neocortical synapses. *Nature* 400: 367–371, 1999.

Fox K. A critical period for experience-dependent synaptic plasticity in rat barrel cortex. *J Neurosci* 12: 1826–1838, 1992.

Fox K. The cortical component of experience-dependent synaptic plasticity in the rat barrel cortex. *J Neurosci* 14: 7665–7679, 1994.

Fox K. The critical period for long-term potentiation in primary sensory cortex. *Neuron* 15: 485–488, 1995.

Fox K. Anatomical pathways and molecular mechanisms for plasticity in the barrel cortex. *Neuroscience* 111: 799–814, 2002.

Fox K, Schlaggar BL, Glazewski S, and O'Leary DD. Glutamate receptor blockade at cortical synapses disrupts development of thalamocortical and columnar organization in somatosensory cortex. *Proc Natl Acad Sci USA* 93: 5584–5589, 1996.

Franklin JL, Fickbohm DJ, and Willard AL. Long-term regulation of neuronal calcium currents by prolonged changes of membrane potential. *J Neurosci* 12: 1726–1735, 1992.

Ganguly K, Kiss L, and Poo M. Enhancement of presynaptic neuronal excitability by correlated presynaptic and postsynaptic spiking. *Nat Neurosci* 3: 1018–1026, 2000.

Garaschuk O, Linn J, Eilers J, and Konnerth A. Large-scale oscillatory calcium waves in the immature cortex. *Nat Neurosci* 3: 452–459, 2000.

Garcia DE, Cavalie A, and Lux HD. Enhancement of voltage-gated Ca^{2+} currents induced by daily stimulation of hippocampal neurons with glutamate. *J Neurosci* 14: 545–553, 1994.

Glazewski S and Fox K. Time course of experience-dependent synaptic potentiation and depression in barrel cortex of adolescent rats. *J Neurophysiol* 75: 1714–1729, 1996.

Hand PJ. Plasticity of the rat cortical barrel system. In: *Changing Concepts of the Nervous System*, edited by Morison AR and Strick PL. New York: Academic, 1982, p. 49-68.

Henderson TA, Woolsey TA, and Jacquin MF. Infraorbital nerve blockade from birth does not disrupt central trigeminal pattern formation in the rat. *Brain Res Dev Brain Res* 66: 146–152, 1992.

Hensch TK, Fagiolini M, Mataga N, Stryker MP, Baekkeskov S, and Kash SF. Local GABA circuit control of experience-dependent plasticity in developing visual cortex. *Science* 282: 1504–1508, 1998.

Hille B. *Ionic Channels of Excitable Membranes* (3rd ed.). Sunderland, MA: Sinauer, 2001.

Huang ZJ, Kirkwood A, Pizzorusso T, Porciatti V, Morales B, Bear MF, Maffei L, and Tonegawa S. BDNF regulates the maturation of inhibition and the critical period of plasticity in mouse visual cortex. *Cell* 98: 739–755, 1999.

Isaac JT, Crair MC, Nicoll RA, and Malenka RC. Silent synapses during development of thalamocortical inputs. *Neuron* 18: 269–280, 1997.

Jahromi BS, Zhang L, Carlen PL, and Pennefather P. Differential time-course of slow afterhyperpolarizations and associated Ca^{2+} transients in rat CA1 pyramidal neurons: further dissociation by Ca^{2+} buffer. *Neuroscience* 88: 719–726, 1999.

Kasper EM, Larkman AU, Lubke J, and Blakemore C. Pyramidal neurons in layer V of the rat visual cortex. II. Development of electrophysiological properties. *J Comp Neurol* 339: 495–518, 1994.

Katz LC and Shatz CJ. Synaptic activity and the construction of cortical circuits. *Science* 274: 1133–1138, 1996.

Kirkwood A, Lee H-K, and Bear MF. Co-regulation of long-term potentiation and experience-dependent synaptic plasticity in visual cortex by age and experience. *Nature* 375: 328–331, 1995.

Lancaster B and Batchelor AM. Novel action of BAPTA series chelators on intrinsic K$^+$ currents in rat hippocampal neurones. *J Physiol* 522: 231–246, 2000.

Laaris N, Carlson GC, and Keller A. Thalamic-evoked synaptic interactions in barrel cortex revealed by optical imaging. *J Neurosci* 20: 1529–1537, 2000.

Lendvai B, Stern E, Chen B, and Svoboda K. Experience-dependent plasticity of dendritic spines in the developing rat barrel cortex in vivo. *Nature* 404: 876–881, 2000.

Li M, Jia M, Fields RD, and Nelson PG. Modulation of calcium currents by electrical activity. *J Neurophysiol* 76: 2595–2607, 1996.

Lipton P, Aitken PG, Dudek FE, Eskessen K, Espanol MT, Ferchmin PA, Kelly JB, Kreisman NR, Landfield PW, Larkman PM, Leybaert L, Newman GC, Panizzon KL, Payne RS, Phillips P, Raley-Susman KM, Rice ME, Santamaria R, Sarvey JM, Schurr A, Segal M, Sejer V, Taylor CP, Teyler TJ, Vasilenko VY, Veregge S, Wu SH, and Wallis R.

Making the best of brain slices: comparing preparative methods. *J Neurosci Methods* 59: 151–156, 1995.

Lo FS and Erzurumlu RS. Neonatal deafferentation does not alter membrane properties of trigeminal nucleus principalis neurons. *J Neurophysiol* 85: 1088–1096, 2001.

Locke RE and Nerbonne JM. Role of voltage-gated K^+ currents in mediating the regular-spiking phenotype of callosal-projecting rat visual cortical neurons. *J Neurophysiol* 78: 2321–2335, 1997.

Lorenzon NM and Foehring RC. The ontogeny of repetitive firing and its modulation by norepinephrine in rat neocortical neurons. *Brain Res Dev Brain Res* 73: 213–223, 1993.

Lorenzon NM and Foehring RC. Alterations in intracellular calcium chelation reproduce developmental differences in repetitive firing and afterhyperpolarizations in rat neocortical neurons. *Brain Res Dev Brain Res* 84: 192–203, 1995.

Lu HC, Gonzalez E, and Crair MC. Barrel cortex critical period plasticity is independent of changes in NMDA receptor subunit composition. *Neuron* 32: 619–634, 2001.

Luthi A and McCormick DA. H-current: properties of a neuronal and network pacemaker. *Neuron* 21: 9–12, 1998.

Magee JC, Avery RB, Christie BR, and Johnston D. Dihidropyridine-sensitive, voltage-gated Ca^{2+} channels contribute to the resting intracellular Ca^{2+} concentration of hippocampal CA1 pyramidal neurons. *J Neurophysiol* 76: 3460–3470, 1996.

Mainen ZF, Maletic-Savatic M, Shi SH, Hayashi Y, Malinow R, and Svoboda K. Two-photon imaging in living brain slices. *Methods* 18: 231–239, 1999.

Mao BQ, Hamzei-Sichani F, Aronov D, Froemke RC, and Yuste R. Dynamics of spontaneous activity in neocortical slices. *Neuron* 32: 883–898, 2001.

Maravall M, Koh IYY, Lindquist WB, and Svoboda K. Experience-dependent changes in basal dendritic branching of layer 2/3 pyramidal neurons during a critical period for developmental plasticity in rat barrel cortex. *Cereb Cortex* DOI: 10.1093/cercor/bhh026, 2004.

Maravall M, Mainen ZF, Sabatini BL, and Svoboda K. Estimating intracellular calcium concentrations and buffering without wavelength ratioing. *Biophys J* 78: 2655–2667, 2000.

McCormick DA, Connors BW, Lighthall JW, and Prince DA. Comparative electrophysiology of pyramidal and sparsely spiny stellate neurons of the neocortex. *J Neurophysiol* 54: 782–806, 1985.

McCormick DA and Pape HC. Properties of a hyperpolarization-activated cation current and its role in rhythmic oscillation in thalamic relay neurons. *J Physiol* 431: 291–318, 1990.

Metherate R and Aramakis VB. Intrinsic electrophysiology of neurons in thalamorecipient layers of developing rat auditory cortex. *Brain Res Dev Brain Res* 115: 131–144, 1999.

Micheva KD and Beaulieu C. Quantitative aspects of synaptogenesis in the rat barrel field cortex with special reference to GABA circuitry. *J Comp Neurol* 373: 340–354, 1996.

Montoro RJ, Lopez-Barneo J, and Jassik-Gerschenfeld D. Differential burst firing modes in neurons of the mammalian visual cortex in vitro. *Brain Res* 460: 168–172, 1988.

Moore CI and Nelson SB. Spatio-temporal subthreshold receptive fields in the vibrissa representation of rat primary somatosensory cortex. *J Neurophysiol* 80: 2882–2892, 1998.

Moyer JR, Thompson LT, and Disterhoft JF. Trace eyeblink conditioning increases CA1 excitability in a transient and learning-specific manner. *J Neurosci* 16: 5536–5546, 1996.

Nelson AB, Krispel CM, Sekirnjak C, and du Lac S. Long-lasting increases in intrinsic excitability triggered by inhibition. *Neuron* 40: 609–620, 2003.

Nick TA and Ribera AB. Synaptic activity modulates presynaptic excitability. *Nat Neurosci* 3: 142–149, 2000.

Nowak LG, Azouz R, Sanchez-Vives MV, Gray CM, and McCormick DA. Electrophysiological classes of cat primary visual cortical neurons in vivo as revealed by quantitative analyses. *J Neurophysiol* 89: 1541–1566, 2003.

Pape HC. Queer current and pacemaker: the hyperpolarization-activated cation current in neurons. *Annu Rev Physiol* 58: 299–327, 1996.

Peters A and Jones EG. Classification of cortical neurons. In: *Cellular Components of the Cerebral Cortex,* edited by Jones EG and Peters A. New York: Plenum, 1984, p. 361-380.

Petersen CC and Sakmann B. Functionally independent columns of rat somatosensory barrel cortex revealed with voltage-sensitive dye imaging. *J Neurosci* 21: 8435–8446, 2001.

Philpot BD, Sekhar AK, Shouval HZ, and Bear MF. Visual experience and deprivation bidirectionally modify the composition and function of NMDA receptors in visual cortex. *Neuron* 29: 157–169, 2001.

Quinlan EM, Philpot BD, Huganir RL, and Bear MF. Rapid, experience-dependent expression of synaptic NMDA receptors in visual cortex in vivo. *Nat Neurosci* 2: 352–357, 1999.

Reece LJ and Schwartzkroin PA. Effects of cholinergic agonists on immature rat hippocampal neurons. *Brain Res Dev Brain Res* 60: 29–42, 1991.

Rice FL and Van der Loos H. Development of the barrels and barrel field in the somatosensory cortex of the mouse. *J Comp Neurol* 171: 545–560, 1977.

Saar D and Barkai E. Long-term modifications in intrinsic neuronal properties and rule learning in rats. *Eur J Neurosci* 17: 2727–2734, 2003.

Sabatini BS, Oertner TG, and Svoboda K. The life-cycle of Ca^{2+} ions in spines. *Neuron* 33: 439–452, 2002.

Schlaggar BL and O'Leary DD. Early development of the somatotopic map and barrel patterning in rat somatosensory cortex. *J Comp Neurol* 346: 80–96, 1994.

Schreurs BG, Gusev PA, Tomsic D, Alkon DL, and Shi T. Intracellular correlates of acquisition and long-term memory of classical conditioning in Purkinje cell dendrites in slices of rabbit cerebellar lobule HVI. *J Neurosci* 18: 5498–5507, 1998.

Schwartz TH, Rabinowitz D, Unni V, Kumar VS, Smetters DK, Tsiola A, and Yuste R. Networks of coactive neurons in developing layer 1. *Neuron* 20: 541–552, 1998.

Schwindt PC, Spain WJ, Foehring RC, Chubb MC, and Crill WE. Slow conductances in neurons from cat sensorimotor cortex in vitro and their role in slow excitability changes. *J Neurophysiol* 59: 450–467, 1988.

Schwindt PC, Spain WJ, Foehring RC, Stafstrom CE, Chubb MC, and Crill WE. Multiple potassium conductances and their functions in neurons from cat sensorimotor cortex in vitro. *J Neurophysiol* 59: 424–449, 1988.

Schwindt PC, Spain WJ, and Crill WE. Effects of intracellular calcium chelation on voltage-dependent and calcium-dependent currents in cat neocortical neurons. *Neuroscience* 47: 571–578, 1992.

Shepherd GMG, Pologruto TA, and Svoboda K. Circuit analysis of experience-dependent plasticity in the developing rat barrel cortex. *Neuron* 38: 277–289, 2003.

Simons DJ. Response properties of vibrissa units in rat SI somatosensory neocortex. *J Neurophysiol* 41: 798–820, 1978.

Simons DJ and Land PW. Early experience of tactile stimulation influences organization of somatic sensory cortex. *Nature* 326: 694–697, 1987.

Sourdet V, Russier M, Daoudal G, Ankri N, and Debanne D. Long-term enhancement of neuronal excitability and temporal fidelity mediated by metabotropic glutamate receptor subtype 5. *J Neurosci* 23: 10238–10248, 2003.

Stern EA, Maravall M, and Svoboda K. Rapid development and plasticity of layer 2/3 maps in rat barrel cortex in vivo. *Neuron* 31: 305–315, 2001.

Svirskis G and Hounsgaard J. Depolarization-induced facilitation of a plateau-generating current in ventral horn neurons in the turtle spinal cord. *J Neurophysiol* 78: 1740–1742, 1997.

Thompson LT, Moyer JR, and Disterhoft JF. Transient changes in excitability of rabbit CA3 neurons with a time course appropriate to support memory consolidation. *J Neurophysiol* 76: 1836–1849, 1996.

Trachtenberg JT, Chen BE, Knott GW, Feng G, Sanes JR, Welker E, and Svoboda K. Long-term in vivo imaging of experience-dependent synaptic plasticity in adult cortex. *Nature* 420: 788–794, 2002.

Turrigiano G, Abbott LF, and Marder E. Activity-dependent changes in the intrinsic properties of cultured neurons. *Science* 264: 974–977, 1994.

van Brederode JF, Foehring RC, and Spain WJ. Morphological and electrophysiological properties of atypically oriented layer 2 pyramidal cells of the juvenile rat neocortex. *Neuroscience* 101: 851–861, 2000.

Velumian AA and Carlen PL. Differential control of three after-hyperpolarizations in rat hippocampal neurones by intracellular calcium buffering. *J Physiol* 517: 201–216, 1999.

Velumian AA, Zhang L, Pennefather P, and Carlen PL. Reversible inhibition of I_k, I_{ahp}, I_h, and I_{Ca} currents by internally applied gluconate in rat hippocampal pyramidal neurons. *Pfluegers* 433: 343–350, 1997.

Viana F, Bayliss DA, and Berger AJ. Postnatal changes in rat hypoglossal motoneuron membrane properties. *Neuroscience* 59: 131–148, 1994.

Wang G-Y, Ratto G-M, Bisti S, and Chalupa LM. Functional development of intrinsic properties in ganglion cells of the mammalian retina. *J Neurophysiol* 78: 2895–2903, 1997.

Welker C. Microelectrode delineation of fine grain somatotopic organization of (SmI) cerebral neocortex in albino rat. *Brain Res* 26: 259–275, 1971.

Welker C and Woolsey TA. Structure of layer IV in the somatosensory neocortex of the rat: description and comparison with the mouse. *J Comp Neurol* 158:437, 1974.

Welker WI. Analysis of sniffing of the albino rat. *Behavior* 22: 223–244, 1964.

Woolsey TA and Van der Loos H. The structural organization of layer IV in the somatosensory region (S1) of mouse cerebral cortex. *Brain Res* 17: 205–242, 1970.

Zhang L, Pennefather P, Velumian AA, Tymianski M, Charlton M, and Carlen PL. Potentiation of a slow Ca-dependent K current by intracellular Ca chelators in hippocampal CA1 neurons of rat brain slices. *J Neurophysiol* 74: 2225–2241, 1995.

Zhang L, Weiner JL, Valiante TA, Velumian AA, Watson PL, Jahromi BS, Schertzer S, Pennefather P, and Carlen PL. Whole-cell recording of the Ca-dependent slow afterhyperpolarization in hippocampal neurones: effects of internally applied anions. *Pfluegers* 426: 247–253, 1994.

Zhang W and Linden DJ. The other side of the engram: experience-driven changes in neuronal intrinsic excitability. *Nat Rev Neurosci* 4: 885–900, 2003.

Zhou FM and Hablitz JJ. Postnatal development of membrane properties of layer I neurons in rat neocortex. *J Neurosci* 16: 1131–1139, 1996.

Zhu JJ and Connors BW. Intrinsic firing patterns and whisker-evoked synaptic responses of neurons in the rat barrel cortex. *J Neurophysiol* 81: 1171–1183, 1999.